Shear flow behaviors of rod-coil diblock copolymers in solution: A nonequilibrium dissipative particle dynamics simulation

Pengxiang Xu, Jiaping Lin, Liquan Wang, and Liangshun Zhang

View Online   Export Citation   CrossMark

Shear flow behaviors of rod-coil diblock copolymers in solution: A nonequilibrium dissipative particle dynamics simulation

Pengxiang Xu, Jiaping Lin,[a)] Liquan Wang, and Liangshun Zhang[a)]
Shanghai Key Laboratory of Advanced Polymeric Materials, State Key Laboratory of Bioreactor Engineering, Key Laboratory for Ultrafine Materials of Ministry of Education, School of Materials Science and Engineering, East China University of Science and Technology, Shanghai 200237, China

We employed the nonequilibrium dissipative particle dynamics method to study the shear flow behaviors of rod-coil diblock copolymers in solutions. The effects of copolymer concentrations and molecular architecture on the rheology are investigated. The simulated results show that the shear flow behaviors change from Newtonian to non-Newtonian when the morphologies transform from micelles to gels by increasing the copolymer concentrations. For the non-Newtonian systems, it was found that the curve of the viscosity versus shear rate is divided into three regions, that is, shear thinning region I, platform region II, and shear thinning region III. From the physical origin, the three-region behavior is governed by the distinct flow behaviors of the rod and coil blocks and their different time scale in response to the shear field. Additionally, by tuning the molecular architectures, the simulated results reveal that the slopes in region I and region III are influenced by the length of rod and coil blocks, respectively. The present research revealed the microscopic origin of the complex rheological properties of rod-coil diblock copolymers in solutions and could provide useful information for preparing functional materials based on block copolymers. *Published by AIP Publishing.*
[http://dx.doi.org/10.1063/1.4982938]

I. INTRODUCTION

Amphiphilic rod-coil diblock copolymers dispersed in selective solvents can exhibit distinct self-assembly behaviors such as forming liquid crystals due to the local ordered packing of rod blocks.[1–5] In these complex structures, each block of rod-coil diblock copolymers exhibits its characteristic conformation feature and shear flow behaviors, which lead to the complexity of rheological properties.[6–8] For this reason, the investigation on the rheology of rod-coil diblock copolymer solutions is essential from the viewpoint of both theoretical research and engineering application. However, so far most of the studies are concerned with the rheological properties of neat flexible or rigid polymeric solutions, while there are limited reports on the rheological properties of rod-coil diblock copolymer solutions. The complex rheological behaviors of rod-coil diblock copolymer solutions under shear flow are still scarcely understood.

For the flexible polymeric solutions, shear thinning is a common feature, where the shear viscosity decreases exponentially with the increasing shear rate due to the stretching and orientation of polymer chains.[9,10] Compared to the flexible polymers, the rigid polymers can only tumble or wag without a stretch in the shear flow field because the rigid chains are at fully extended state.[11,12] Burghardt *et al.* conducted a series of experiments on the rheology of the solutions of rigid poly(γ-benzyl glutamate)[13,14] and hydroxypropylcellulose.[15,16] They

found that the rigid polymeric solutions generally exhibit a "polydomain" texture, and the shear thinning curve presents three regions, which is in agreement with the Larson-Doi model.[12] When a rigid molecule and a flexible molecule are covalently bonded together as a rod-coil diblock copolymer, the different flow behaviors of rigid and flexible molecules lead to the complex rheological properties.[6,17–20] Ober and co-workers reported that changing the molecular architecture from neat rigid homopolymers to rod-coil diblock copolymers induces a decrease in the complex viscosity, which is attributed to the presence of a coil block as the second block and the effect of topological constrains on molecular relaxation.[6] Jeong *et al.* recently synthesized a series of poly(ethylene glycol)-poly(*L*-alanine) block copolymers and investigated the effect of block length on the rheological properties.[19] They found that the sol-gel transition temperature, where a crossover of storage modulus and loss modulus takes place, decreases by increasing the molecular weight ratio of the rod block to the coil block. Despite these studies, the microscopic origin of the complex rheological behaviors of the rod-coil diblock copolymer solutions is still one particular aspect concerned in the polymeric experiments.

Apart from the experiments, the theoretical simulation method can provide specific information which is difficult to be obtained from the experiments. Equilibrium and non-equilibrium molecular dynamics (MD) simulations are widely used to study the mechanical and rheological properties of both untangled and entangled linear polymers.[21–27] Berker *et al.* adopted non-equilibrium molecular dynamics (NEMD) to simulate the rheological properties of *n*-Hexadecane melts.[22] They found that the NEMD can well simulate the non-Newtonian behaviors such as shear thinning, shear dilatancy,

a)Authors to whom correspondence should be addressed. Electronic addresses: jlin@ecust.edu.cn and zhangls@ecust.edu.cn. Tel.: +86-21-64253370.

and normal stress effects. However, the NEMD could not accurately simulate the rheology of polymeric solutions because hydrodynamic interactions are not considered in NEMD.[28] Later, dissipative particle dynamics (DPD) method was developed as an effective mesoscopic method to simulate the simple and complex fluids,[29–32] and the non-equilibrium simulation technique was further coupled to the DPD method to simulate the flow behavior of polymeric solutions.[33–45] For example, Ganesan and co-workers adopted a non-equilibrium oscillatory shear method based on the DPD simulations to study the linear viscoelastic of gel systems formed by amphiphilic ABA triblock copolymers dispersed in solvents.[38] Their results are in good agreement with other theoretical predictions and experimental findings. The success of non-equilibrium DPD simulation makes it ready to be extended to predict the rheology of rod-coil diblock copolymer solutions.

In the present work, we constructed a model of rod-coil diblock copolymers in solutions to investigate their shear flow behaviors by taking advantages of the DPD and the non-equilibrium simulations. Such methods are applied to investigate the effects of copolymer concentration and molecular architecture on the rheological properties of these copolymer solutions. Beyond obtaining the equilibrium structures, we observed that the flow curves are divided into three regions in the concentrated solutions by using non-equilibrium DPD simulations. Then, we aimed to reveal the microscopic origin of the three-region behaviors in the flow curves of rod-coil diblock copolymer solutions, which cannot be resolved by equilibrium simulations and experimental measurements. It was discovered that the three-region behavior is governed by the distinct flow behaviors of the rod and coil blocks and their different time scales in response to the shear field.

II. METHODS AND MODEL

A. DPD method

Dissipative particle dynamics (DPD) is a typical coarse-grained simulation method originally proposed by Hoogerbrugge and Koelman.[29,30] In the DPD simulations, a particle having mass M represents a cluster of atoms or segments rather than an individual atom. These particles interact with each other through soft particle-particle interactions. The movement of the particles can be realized by solving the Newton's equations of motion

$$\frac{d\mathbf{r}_i}{dt} = \mathbf{v}_i, \quad M_i \frac{d\mathbf{v}_i}{dt} = \mathbf{f}_i, \tag{1}$$

where M_i, $\mathbf{r}_i$, $\mathbf{v}_i$, and $\mathbf{f}_i$ denote the mass, position, velocity, and the total force acting on the ith particle, respectively. The total force $\mathbf{f}_i$ is divided into three parts, the conservative force $\left(\mathbf{F}_{ij}^C\right)$, dissipative force $\left(\mathbf{F}_{ij}^D\right)$, and random force $\left(\mathbf{F}_{ij}^R\right)$,

$$\begin{aligned} \mathbf{f}_i &= \sum_{j \neq i} \mathbf{F}_{ij}^C + \mathbf{F}_{ij}^D + \mathbf{F}_{ij}^R, \\ \mathbf{F}_{ij}^C &= a_{ij} \sqrt{\omega(r_{ij})} \hat{\mathbf{r}}_{ij}, \\ \mathbf{F}_{ij}^D &= -\Gamma \omega(r_{ij})(\hat{\mathbf{r}}_{ij} \cdot \mathbf{v}_{ij}) \hat{\mathbf{r}}_{ij}, \\ \mathbf{F}_{ij}^R &= \sigma \sqrt{\omega(r_{ij})} \theta_{ij} \hat{\mathbf{r}}_{ij}, \end{aligned} \tag{2}$$

where $\mathbf{r}_{ij} = \mathbf{r}_i - \mathbf{r}_j$, $r_{ij} = |\mathbf{r}_{ij}|$, $\hat{\mathbf{r}}_{ij} = \mathbf{r}_{ij}/r_{ij}$, and $\mathbf{v}_{ij} = \mathbf{v}_i - \mathbf{v}_j$. The weight function $\omega(r_{ij})$ equals to $(1 - r_{ij}/r_c)^2$ with a cut-off distant r_c, according to the study of Groot and Warren.[28] a_{ij}, Γ, σ, and θ_{ij} are repulsive parameter, friction coefficient, noise amplitude, and Gaussian random variable, respectively. To keep the temperature of system constant, Γ and σ satisfy the fluctuation-dissipative theorem as $\sigma^2 = 2\Gamma k_B T$, where k_B and T are, respectively, the Boltzmann constant and the absolute temperature.

We constructed a DPD model of rod-coil diblock copolymers $R_m C_n$ with a solvophilic coil block (denoted by C) and a solvophobic rod block (R) surrounded by solvent particles (S), as shown in Figure 1(a). The lengths of rod and coil blocks are, respectively, indicated by m and n. For a copolymer chain, neighbor particles are connected by a harmonic spring potential

$$U_{ij}^{b_1} = \frac{1}{2} C_1 \left(r_{ij} - r_{eq}\right)^2. \tag{3}$$

In this work, the spring constant is $C_1 = 100.0\varepsilon/r_c^2$ and the equilibrium length of spring is $r_{eq} = 0.7r_c$, where the ε is energy unit. To ensure the rigidity of rod blocks, three additional potentials are applied. The first one is the angle bending potential defined by each of the three connected particles,

$$U_{angle}(\theta) = \frac{1}{2} k_\theta (\cos \theta - \cos \theta_0)^2, \tag{4}$$

where k_θ is the angle spring constant and θ_0 is the equilibrium angle. We choose $\theta_0 = 180°$ to realize the linear rod blocks and $k_\theta = 20\varepsilon$. Two suppositional harmonic spring potentials are added to the rod blocks, as illustrated in Figure 1(a). They are
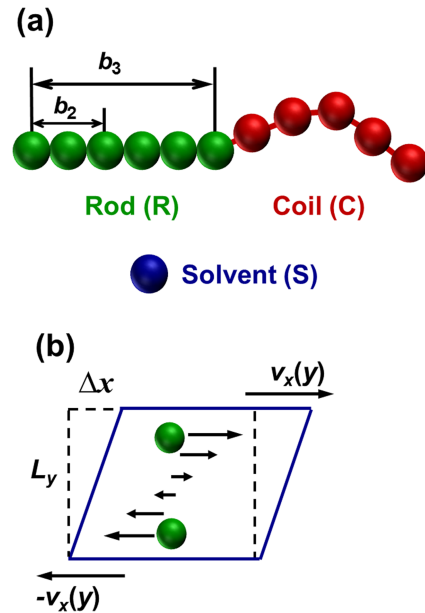
(a)

(b)

FIG. 1. (a) Model of an amphiphilic rod-coil diblock copolymer $R_m C_n$. The green, red, and blue beads represent the rod block, coil block, and solvents, respectively. Two suppositional harmonic spring potentials are added to the rod blocks. They are b_2 for the first and the third particles in every three connected particles and b_3 for the head and the tail particles of an entire rod block. (b) Schematic representation of the simulation box projecting on the xy-plane. The change of box shape from orthogonal to triclinic induces shear flow $\mathbf{v}_x(y)$ in the x direction and velocity gradient in the y direction. Δx and L_y represent the displacement in x direction and the edge length in the y direction, respectively.

$U_{ij}^{b_2}$ for the first and the third particles in every three connected particles and $U_{ij}^{b_3}$ for the head and the tail particles of an entire rod block,[20]

$$U_{ij}^{b_2} = \frac{1}{2}C_2\left(r_{ij} - r_{eq}^{b_2}\right)^2, \quad U_{ij}^{b_3} = \frac{1}{2}C_3\left(r_{ij} - r_{eq}^{b_3}\right)^2. \quad (5)$$

Here, the spring constants are $C_2 = C_3 = 100\varepsilon/r_c^2$ and the equilibrium lengths of spring are $r_{eq}^{b_2} = 1.4r_c$ and $r_{eq}^{b_3} = (m - 1) \times 0.7r_c$, where m is the particle amount of a single rod block.

In the DPD simulation method, reduced units are adopted for all physical quantities.[28] The units of mass, length, and energy are defined by M, r_c, and ε, respectively. The time unit τ can be obtained by $\tau = (Mr_c^2/\varepsilon)^{1/2}$, and its real value can be estimated by matching the simulated lateral diffusion coefficient to the experimental measured value.[28]

B. Nonequilibrium simulation

To simulate the polymeric solutions subjected to an external shear flow field, we employed the SLLOD algorithm coupled with Lee-Edwards periodic boundary conditions. Although the SLLOD algorithm could lead to artefacts of the linear shear profile in the inhomogeneous system, it is acceptable when one focuses on the bulk properties in the solutions far from the surface.[33] The SLLOD algorithm generates the following equations of motion:

$$\frac{d\mathbf{r}_i}{dt} = \mathbf{v}_i + \mathbf{e}_x\dot{\gamma}r_{i,y},$$
$$M_i\frac{d\mathbf{v}_i}{dt} = \mathbf{f}_i - M_i\mathbf{e}_x\dot{\gamma}v_{i,y}, \quad (6)$$

where $\dot{\gamma}$ is the shear rate of the external shear flow defined by $\dot{\gamma} = \partial v_x/\partial r_y$ and $\mathbf{e}$ is unit vector. The subscripts x, y denote the components of a vector. The velocity of ith particle is divided into two parts, that is, the peculiar velocity $\mathbf{v}_i$ representing the random thermal motions and the shear flow velocity $\mathbf{e}_x\dot{\gamma}r_{i,y}$ relating to the external disturbance strength.

Under the shear flow, the viscosity of the copolymer solutions is calculated as

$$\eta = -\frac{\sigma_{xy}(\dot{\gamma})}{\dot{\gamma}}. \quad (7)$$

Here, the stress σ_{xy} is obtained using the tensor version of the virial theorem

$$\boldsymbol{\sigma} = \frac{1}{V}\left\langle \sum_i M_i\mathbf{v}_i\mathbf{v}_i + \frac{1}{2}\sum_{i\neq j}\mathbf{r}_{ij}\mathbf{F}_{ij} \right\rangle, \quad (8)$$

where V denotes the volume of the system and the angular bracket represents ensemble average.

C. Model and condition

All the simulations were performed in a triclinic (non-orthogonal) box, where three tilt factors T_{xy}, T_{xz}, and T_{yz} represent the amount of displacement applied to the faces of an orthogonal box to transform it into the parallelepiped. For instance, the T_{xy} equals to the displacement Δx in the x direction divided by the box edge length L_y in the y direction, i.e., $T_{xy} = \Delta x/L_y$. The definitions of the other tilt factors, T_{xz} and T_{yz}, are similar to that of T_{xy}. The triclinic simulation box turns back to be the orthogonal one when all the

tilt factors are set to be zero. We performed all of the simulations in an initially orthogonal box of $30 \times 30 \times 30\ r_c^3$, containing 81 000 coarse-grained particles. The friction coefficient Γ and the noise amplitude σ were, respectively, set as $4.5\ \varepsilon\tau/r_c^2$ and $3.0\ \varepsilon\tau^{1/2}/r_c$, and thus the temperature was kept constant as $k_BT = 1.0\varepsilon$. The velocity-Verlet algorithm was used to integrate the equations of motion with a time step of $\Delta t = 0.04\tau$. After the equilibrium structures were achieved during 6×10^5 steps, shear flow simulations were performed by continuously increasing the tilt factor T_{xy} of the computational box. As schematically illustrated in Figure 1(b), the particles motioned in the x direction following the box deformation from the orthogonal box to the triclinic one. Especially, the particles with a larger y coordinate motioned faster than those with a smaller y coordinate, which gave rise to the linear velocity gradient in the y direction. As the Lee-Edwards periodic boundary conditions were imposed on the simulation box, the triclinic box with $T_{xy} = 1/2$ was equivalent to that with $T_{xy} = -1/2$. When T_{xy} exceeded 1/2, the simulation box was re-shaped to the other case (i.e., $T_{xy} = -1/2$) and the simulation continued with T_{xy} further increasing from $-1/2$.

III. RESULTS AND DISCUSSION

In this work, we considered the systems of R_mC_n rod-coil diblock copolymers dispersed in solvents selective to coil blocks. First, we applied the DPD method outlined above to examine the equilibrium structures of copolymer solutions with various copolymer concentrations, lengths of rod blocks, and lengths of coil blocks. After obtaining the equilibrium structures, we used the non-equilibrium DPD method to explore the rheological properties of R_mC_n solutions under steady shear flow.

A. Effect of copolymer concentration

In this subsection, we focused on the effect of copolymer concentrations (denoted by ϕ) on the self-assembly and shear flow behaviors of rod-coil diblock copolymer solutions. The concentration ϕ is defined as the ratio of copolymer particle amounts ($N_R + N_C$) to the total particle amounts ($N_R + N_C + N_S$). The repulsive parameters in Equation (2) are set as $a_{RC} = 80$, $a_{RS} = 60$, and $a_{CS} = 25$, where R, C, and S denote the rod blocks, coil blocks, and solvent particles, respectively. The parameters between the like particles a_{RR}, a_{CC}, and a_{SS} are 25. We set the repulsive parameter a_{RC} between the rod and coil blocks larger than the value of a_{RS} between the rod blocks and the solvent particles, in order to achieve the strong separation of the rod and coil blocks in the domains and decouple the influences of rod and coil blocks on the rheological properties.

Figure 2 shows the typical equilibrium structures self-assembled from R_6C_4 diblock copolymer solutions with various concentrations ϕ. As shown in Figure 2(a), the amphiphilic rod-coil diblock copolymers form spherical or rod-like micelles when the ϕ is low (i. e., $\phi = 0.1$). In the micelles, the solvophobic rod blocks located in the core domain are surrounded by the solvophilic coil blocks. By increasing ϕ to 0.2, the rod-like micelles become longer and are transformed to the wormlike micelles (see Figure 2(b)). The
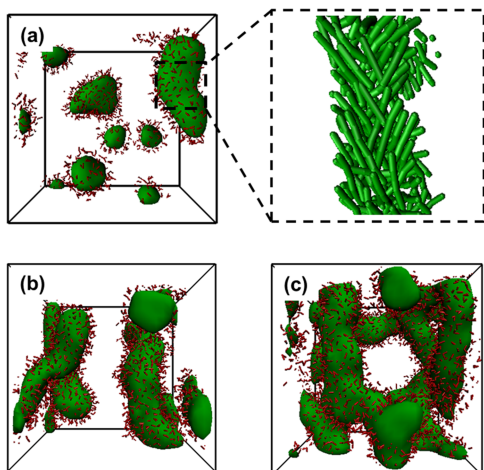
FIG. 2. Self-assembled structures of R_6C_4 rod-coil diblock copolymers dispersed in the solvents selective to coil blocks at various copolymer concentrations: (a) $\phi = 0.1$, (b) $\phi = 0.2$, and (c) $\phi = 0.3$. In panel (a), the enlarged view indicates the packing of rod blocks. The green and red colors are, respectively, assigned to R and C blocks, while the solvents are omitted for clarity.

formation of wormlike structures coincidences with some available experimental findings, where long nanofibers,[3,46] twisted string structures,[7,47] and ribbons are identified.[5] Further increasing ϕ to 0.3, the wormlike micelles are linked with each other, leading to the production of gel-like network structures (see Figure 2(c)).

Analyzing the equilibrium structures revealed that the rod blocks pack twisting along the long axis of rod-like micelles with a tilting angle (see the enlarged view of Figure 2(a)) due to the competition between the anisotropy of rod blocks and the immiscibility of different blocks. The twisted packing manner of rod blocks results in the formation of rod-like or wormlike micelles, which is in accordance with our previous findings.[48–50] To reduce the interface energy, the twisted packing rod blocks are shielded from the solvents by the coil blocks surrounding them. However, in the samples of asymmetric R_6C_4 copolymers where the coil blocks are shorter than the rod blocks, the solvophobic rod blocks could not be completely protected by the solvophilic coil blocks, leading to some exposure of rod blocks to the solvents. By increasing ϕ to 0.3, the energetic cost of micellar lateral is compensated

by linking each of the wormlike micelle with the other, leading to the formation of gel-like network structures. The simulated result (i.e., increasing copolymer concentrations induces the gelation of micellar solutions) is inline with the experimental findings.[4,7,51] For example, Deming's group prepared an aqueous solution of amphiphilic poly-L-lysine-*b*-poly-L-leucine diblock copolymer.[7] They confirmed that the self-assembled nanofibers or ribbons of rod-coil copolymers interconnect with each other to form the percolated network structures with elastic properties and divergent zero shear viscosity.

To investigate the rheological properties of the rod-coil diblock copolymer solutions, we then carried out the non-equilibrium DPD simulations of the R_6C_4 solutions subjected to the steady shear flow. Figure 3(a) shows the stress-strain curves of R_6C_4 solutions with $\phi = 0.1$, $\phi = 0.2$, $\phi = 0.3$, and $\phi = 0.4$. All of the simulations are under the steady shear flow with the same constant shear rate of $\dot{\gamma} = 0.06\tau^{-1}$. It can be seen from Figure 3(a) that all the samples exhibit the similar stress-strain behaviors despite their different shear stress quantities. The stresses gradually increase in the region of low shear strain $\gamma < 0.8$, then decrease to a certain value at the intermediate strain $0.8 < \gamma < 2.0$, and lastly maintain a constant value with a weak oscillatory beyond $\gamma > 2.0$. Taking the system with $\phi = 0.4$ as an example, we discuss the relation between the shear flow behaviors and the structural evolution in details.

The representative morphology snapshots are shown in Figure 3 for the encircled points with labels (i), (ii), (iii), and (iv) in Figure 3(a). It can be seen that the self-assembled structure is changed from the network structure to the parallel stacking cylinders as γ increases from 0 to 0.8. The cylinders have a tilt angle $\theta_{c,x}$ between the main axis of cylinders and the flow direction, which is schematically illustrated in the inset of Figure 3(b). In this region of $\gamma < 0.8$, the morphological transition from the equilibrium structure increases the interface energy, leading to the gradual increase of shear stress. At intermediate shear strain, $0.8 < \gamma < 2.0$, the $\theta_{c,x}$ continuously decreases (see Figure 3(b)). Even at $\gamma = 2.0$, the $\theta_{c,x}$ approaches zero, indicating that the cylinders are almost parallel to the flow direction. Meanwhile, the molecular orientation of copolymers also changes during the shear flow (discuss later in details). The orientation changes of the cylindrical main axis and the copolymer molecules reduce the resistance
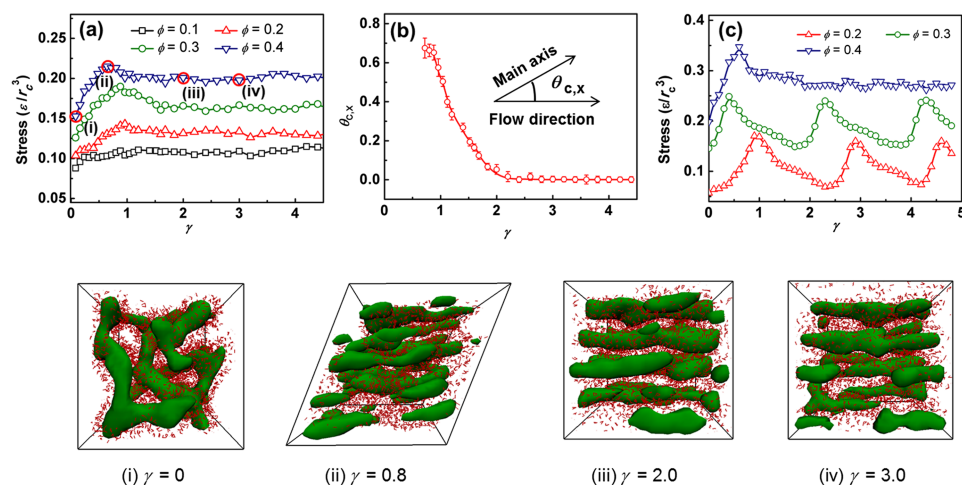

FIG. 3. (a) Stress-strain curves of R_6C_4 rod-coil diblock copolymer solutions with various concentrations ϕ under steady shear flow of $\dot{\gamma} = 0.06\tau^{-1}$. Representative morphology snapshots for the encircled points with labels (i), (ii), (iii), and (iv) are shown for samples of $\phi = 0.4$ at $\gamma = 0$, $\gamma = 0.8$, $\gamma = 2.0$, and $\gamma = 3.0$, respectively. (b) The mean angle $\theta_{c,x}$ between the main axis of cylinders and the flow direction with respect to the shear strain. The inset shows the schematic illustration of the angle $\theta_{c,x}$. (c) Stress-strain curves of R_{10} rigid homopolymer solutions with various ϕ under the steady shear flow of $\dot{\gamma} = 0.06\tau^{-1}$.

(i) $\gamma = 0$ (ii) $\gamma = 0.8$ (iii) $\gamma = 2.0$ (iv) $\gamma = 3.0$

to the shear flow, and thus the stress decreases at intermediate strain, $0.8 < \gamma < 2.0$. The R_6C_4 solutions with $\phi = 0.1$, $\phi = 0.2$, and $\phi = 0.3$ were also examined. It was found that the R_6C_4 solutions with different ϕ show almost the same structural evolutions: the morphologies are transformed from equilibrium structures (i.e., rod-like micelles for $\phi = 0.1$, wormlike micelles for $\phi = 0.2$, and network structures for $\phi = 0.3$) to cylinders, then the cylinders orientate to the flow direction. When $\gamma > 2.0$, the systems achieve the steady state that the morphology keeps almost unchanged, and the stress maintain a constant value with a weak oscillatory which is common in rigid molecule solutions.[12,13,52]

As a reference simulation, a rigid homopolymer R_{10} sample was constructed. The stress-strain curves of R_{10} solutions with various polymer concentrations were presented in Figure 3(c). Compared to Figure 3(a), the oscillatory in the stress-strain curves of R_{10} rigid homopolymer solutions is stronger than that of R_6C_4 diblock copolymer solutions (note that the scale of the vertical axis in Figure 3(a) is larger than that in Figure 3(c)). According to the Leslie-Ericksen theory, the oscillatory in stress-strain curve originates from the tumbling and wagging of rigid molecules during the shear flow rather than alignment,[11] which were widely studied by the experiments[13–16] and the theoretical simulations.[53–56] As mentioned above, the R_6C_4 solutions form the core-shell structures, where the rod blocks are located in the cores surrounded by the coil blocks. Therefore, under the shear flow, the rod blocks can only tumble or wag in the confined space consisting of the coil blocks. In addition, one end of the rod block is not free due to bonding to the coil blocks. Both the confinement and the connectivity weaken the capability of tumbling and wagging of the rod blocks. This could be the reason why the oscillatory in stress-strain curves for R_6C_4 rod-coil diblock copolymer solutions is weaker than that for R_{10} rigid homopolymer solutions.

To explicitly show the evidence of tumbling of rods in the systems of rod-coil diblock copolymers, we tracked the x-component $u_x(t)$ of the direction vector of a representative rod. Figure S1 of supplementary material shows the temporal evolution of $u_x(t)$ for a representative rod in the R_6C_4 system at $\phi = 0.4$ under $\dot{\gamma} = 0.01\tau^{-1}$. It can be seen that $u_x(t)$ periodically varies around its equilibrium position, indicating that the rods gradually tumbled.

Due to the oscillatory in the stress-strain curves, the time average of stress after the steady state is achieved, substituting the ensemble average of stress in Equation (8), is used to calculate the apparent shear viscosity. All the four R_6C_4 solutions with various ϕ were calculated under the shear rate scanning, and the curves of apparent viscosity versus shear rate were plotted in Figure 4. As shown in Figure 4(a), the shear viscosity remains almost constant for $\phi = 0.1$, while shear thinning is observed for $\phi \geq 0.2$. These phenomena manifest the fact that a transition from Newtonian to non-Newtonian flow behavior takes place between $\phi = 0.1$ and $\phi = 0.2$. For the non-Newtonian systems with $\phi \geq 0.2$, the viscosity-shear rate curves can be divided into three regions with respect to the shear rate. Figure 4(b) shows the schematic illustration of the three regions, that is, shear thinning in region I ($\dot{\gamma} < 0.01\tau^{-1}$), platform in region II ($0.01\tau^{-1} < \dot{\gamma} < 0.05\tau^{-1}$), and shear
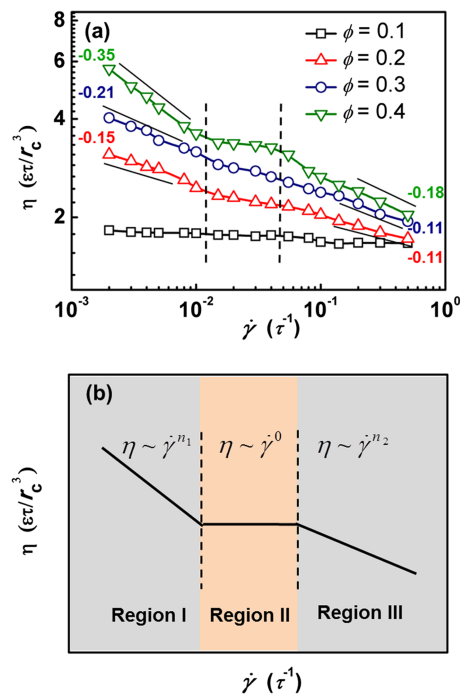

FIG. 4. (a) The apparent viscosity versus shear rate for R_6C_4 diblock copolymer solutions with various copolymer concentrations of $\phi = 0.1$, $\phi = 0.2$, $\phi = 0.3$, and $\phi = 0.4$. The numbers in the plot indicate the slopes of power-law shear thinning regions. (b) Schematic illustration of the three-region behavior, that is, shear thinning in region I, platform in region II, and shear thinning in region III.

thinning in region III ($\dot{\gamma} > 0.05\tau^{-1}$). The slopes of the curves in region I are -0.15, -0.21, and -0.35 for $\phi = 0.2$, $\phi = 0.3$, and $\phi = 0.4$, respectively. All of the three slopes in region I are larger than those in region III (-0.11, -0.11, and -0.18 for $\phi = 0.2$, $\phi = 0.3$, and $\phi = 0.4$, respectively). The three-region flow behavior in the simulated non-Newtonian R_6C_4 systems is similar to that of lyotropic liquid crystal polymers reported by Burghardt *et al.*[16] Their work shows that the flow behavior in regions II and III is similar to that of the traditional flexible polymeric solutions, while the divergence of viscosity-shear rate curves in region I has arisen from the distortional elasticity of nematic phase. In Subsection III B, we discuss the origin of the three-region behavior of rod-coil diblock copolymer solutions in details.

B. Three-region flow behavior

The complex features of three-region flow behaviors of rod-coil copolymer solutions could originate from the different responses to the shear flow of respective blocks. It is well known that the rod blocks can only rotate, while the coil blocks can stretch from random coil conformation to more extended conformations during the shear flow. To get deeper insight into the influences of rod and coil blocks on the rheological properties, we define two molecular parameters to characterize the stretching behaviors of coil blocks and the orientation behaviors of rod blocks. They are the stretching degree (S_d) of coil blocks and the normalized length projections (p_α) on α direction of rod blocks, given by

$$S_d = \frac{R_C}{L_C}, \quad p_\alpha = \frac{L_{R,\alpha}}{L_R}, \tag{9}$$

where L_C and L_R are the contour length of coil and rod blocks, respectively. R_C is the root-mean-square end-to-end distance of the coil blocks and $L_{R,\alpha}$ denotes the length of rod blocks projecting on the α direction. The p_α can be divided into three parts, that is, projections on the flow direction (p_x), velocity gradient direction (p_y), and neutral direction (p_z). The temporal evolutions of p_α and S_d of the R_6C_4 solutions with $\phi = 0.4$ in the presence of shear flow were summarized in Figure 5. At the initial state (i.e., $t = 0\tau$), the value of p_y is slightly larger than those of p_x and p_z, implying that the rod blocks are aligned almost uniformly with a slight tilt to the y-direction. At low shear rate of $\dot\gamma = 0.01\tau^{-1}$, p_x increases slightly and p_y maintains a constant value (see Figure 5(c)), while the stretching degree S_d slightly increases to 0.342 at the time of 210τ then keeps unchanged. However, at a high shear rate of $\dot\gamma = 0.4\tau^{-1}$, as shown in Figure 5(b), p_x increases rapidly and becomes much larger than p_y and p_z, suggesting
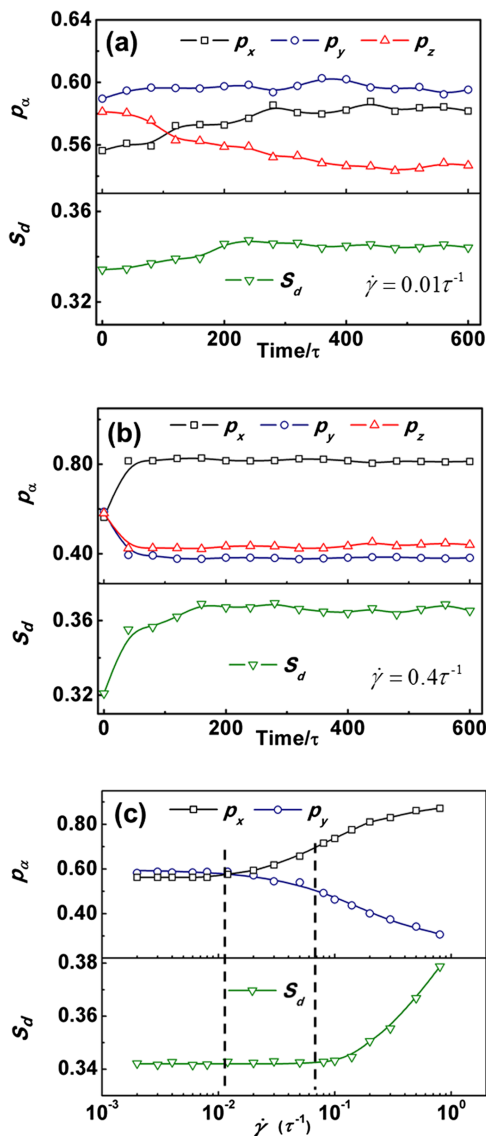

FIG. 5. The temporal evolution of mean projections p_α of rod blocks on the x direction (black), y direction (blue), and z direction (red) and stretching degree S_d of coil blocks (green) at (a) low shear rate $\dot\gamma = 0.01\tau^{-1}$ and (b) high shear rate $\dot\gamma = 0.4\tau^{-1}$. (c) Plots of p_x, p_y, and S_d as a function of the shear rate. The simulated systems are R_6C_4 diblock copolymer solutions with concentration of $\phi = 0.4$.

that the rod blocks are highly oriented along the flow direction. At the same time, the S_d is also shifted towards a higher value of 0.363.

With these two parameters, i.e., normalized length projections p_α of rod blocks and stretching degree S_d of coil blocks, we further explored the origin of three regions in the curve of viscosity versus shear rate for the representative R_6C_4 solutions with $\phi = 0.4$. The plots of p_x, p_y, and S_d as a function of shear rate are presented in Figure 5(c). In the region I of $\dot\gamma < 0.01\tau^{-1}$, p_x, p_y, and S_d maintain invariable, indicating that the coil blocks are not stretched and the rod blocks are not oriented along the flow direction. The shear thinning in region I could be arisen from the relaxation of the local liquid-crystal structures known as "polydomain" structures proposed by Burghardt and Fuller.[13] In this region, the flow is not strong enough to disturb the microstructure, and the plastic flow (i.e., shear thinning) takes place. In the region II of $0.01\tau^{-1} < \dot\gamma < 0.05\tau^{-1}$, S_d is unchanged, while p_x and p_y start increasing and decreasing, respectively (see Figure 5(c)). In this region, the equilibrium structure was disturbed by the shear flow and transformed to cylinders, as can be seen in the morphological snapshots of Figure 3. On the one hand, the shear field results in the alignment of rod blocks along the flow direction as p_x increases. This alignment behavior causes the loss of distortional elasticity, resulting in the decrease of the viscosity. On the other hand, this arrangement mode of rod blocks causes the decrease of cross section diameter of cylinders as p_y decreases (see Figure 5(c)), and thus the interface area and interface energy increase. The increase of the interface energy can enhance the resistance of copolymers to the shear flow. The interplay of these two factors results in the Newtonian platform in region II. With further increasing the shear rate to $\dot\gamma > 0.05\tau^{-1}$, p_x approaches to a high value of 0.86 and S_d starts increasing, indicating that the rod blocks are highly oriented and the coil blocks start stretching. As a result, the resistance of polymers to the shear dramatically decreases, and therefore the shear thinning behavior recovers and the power-law shear thinning region III appears.

To deepen the understanding of microscopic origin of the crossovers between distinct regions of non-Newtonian behaviors, we also examined the rotational relaxation time of the rods and the Rouse time of the coils. The rotational relaxation time τ_r of the rods was obtained by the rotational diffusion process at the equilibrium state. The τ_r is related to the mean square displacement (MSD) of the direction vector $\mathbf{u}(t)$ of rods, given by[57]

$$\left\langle [\mathbf{u}(t) - \mathbf{u}(0)]^2 \right\rangle \propto 2(1 - \exp(-t/\tau_r)). \tag{10}$$

Similarly, the Rouse time τ_1 of the coils was estimated by the time correlation function (TCF) of the end-to-end vectors $\mathbf{P}(t)$ of coil blocks, satisfying the relationship[57]

$$\langle \mathbf{P}(t) \cdot \mathbf{P}(0) \rangle \propto \exp(-t/\tau_1). \tag{11}$$

Figure S2 of the supplementary material shows the plots of MSD and TCF as a function of the simulation time for the R_6C_4 solutions at $\phi = 0.4$. In the plots, the solid lines are the theoretical fitting curves according to Equations (10) and (11). We can deduce that the rotational relaxation time of the rods and the Rouse time of the coils are $\tau_r = 136\tau$ and $\tau_1 = 25\tau$,

respectively. These values are close to the time scales of 100τ and 20τ, which correspond to the crossover shear rates of $0.01\tau^{-1}$ and $0.05\tau^{-1}$.

In order to study the combined influences of the rod and coil blocks on the rheological properties, we compared the viscosity-shear rate curves of three solutions (see Figure 6(a)), which are R_6C_4 rod-coil diblock copolymer solutions, A_6B_4 coil-coil diblock copolymers in B-selective solvents, and R_{10} rigid homopolymers in good solvents. The copolymer concentrations are fixed at $\phi = 0.4$. The viscosity-shear rate curves for solutions with a lower concentration ($\phi < 0.4$) are not shown due to the strong oscillatory for rigid homopolymer solutions (see Figure 3(b)). At a low shear rate, the viscosity of A_6B_4 coil-coil diblock copolymer solutions remains constant (i.e., zero-shear rate viscosity), while both the R_{10} and R_6C_4 solutions show shear thinning behaviors. However, by increasing the shear rate, both the A_6B_4 and R_{10} solutions do not show the three-region behavior in the viscosity-shear rate curves. In addition, p_x and S_d as a function of the shear rate for these solutions were presented in Figure 6(b). It can be seen that the stretching behavior of A_6B_4 solutions is similar to the traditional flexible polymeric solutions. Meanwhile, in the range of $10^{-3}\tau^{-1} < \dot{\gamma} < 1\tau^{-1}$, p_x of R_{10} homopolymer solutions gradually increases, and thus the viscosity gradually decreases without the existence of platform region II in the viscosity-shear rate curve of R_{10} solutions.

From the comparison of R_6C_4, A_6B_4, and R_{10} solutions above, we can come to a conclusion that the three-region behavior is a characteristic of rod-coil copolymer solutions.

It should be noted that the three-region behavior can also be found in some rigid polymeric solutions in experiments.[11–14] In the simulated R_{10} solutions, the absence of region II could originate from the fact that the region II is too narrow at the present parameters employed. From the analysis of Figure 5(c), we learned that the three regions in the viscosity-shear rate curves of rod-coil diblock copolymer solutions originate from the difference of the time scales between the tumbling-alignment transition of the rod blocks and the stretching behavior of the coil blocks. During the shear rate scanning, the rod blocks respond to the shear flow more easily and start orienting along the flow direction at lower shear rate, and the stretching behavior of coil blocks lags behind the orientation behavior of the rod blocks by one order of magnitude, leading to the complex three-region behaviors.

C. Effects of molecular architecture

As illustrated above, the coil blocks prefer to randomly pack in the equilibrium structures, while the rod blocks have priority to form parallel packed structures. Furthermore, the rod and coil blocks respond to the shear flow at different time scales. Such computational results suggest that the molecular architecture, such as the lengths of rod and coil blocks, plays an important role in influencing the rheological properties. In this subsection, we systemically tune the lengths of rod and coil blocks to examine the influence of such variations on the shear flow behaviors of rod-coil diblock copolymer solutions.

Figure 7(a) shows the viscosity-shear rate curves for the R_6C_n diblock copolymer solutions under steady shear flow, where the copolymer concentrations are fixed at $\phi = 0.4$. Three
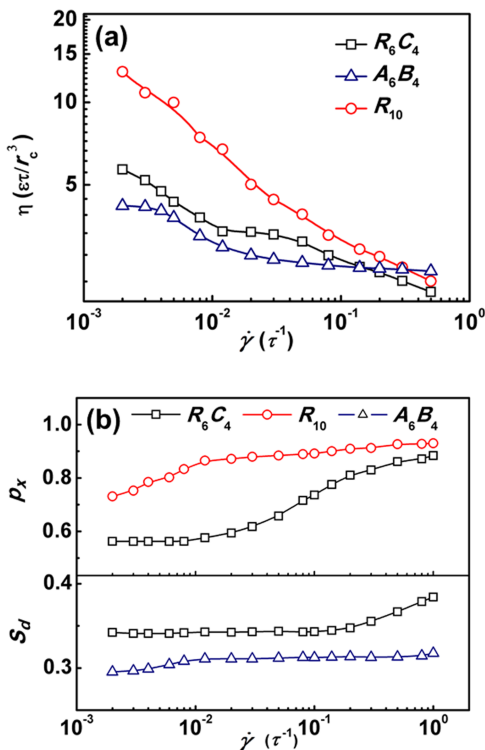
FIG. 6. (a) Viscosity-shear rate curves for R_6C_4 rod-coil diblock copolymer solutions, A_6B_4 coil-coil diblock copolymer solutions, and R_{10} rigid polymeric solutions. (b) p_x as a function of shear rate for the R_{10} and R_6C_4 solutions in the upper panel, and S_d as a function of shear rate for the A_6B_4 and R_6C_4 solutions in the bottom panel. The polymer concentrations are fixed at $\phi = 0.4$ for all the systems.
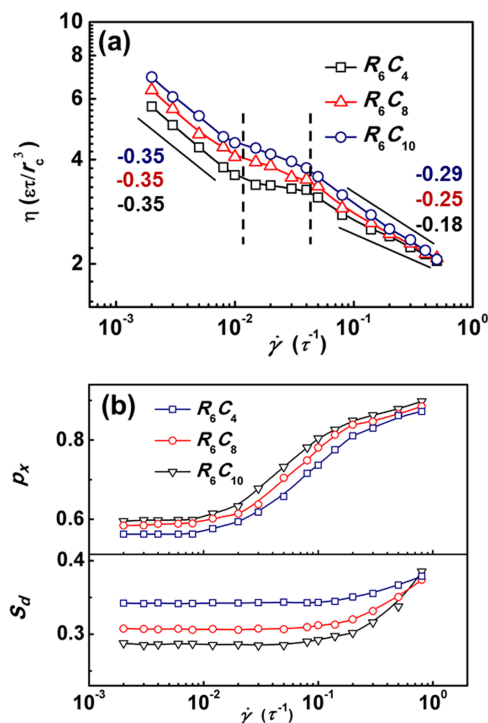
FIG. 7. (a) Shear viscosity as a function of the shear rate for the solutions of R_6C_n diblock copolymers with various lengths of coil blocks at $\phi = 0.4$. The numbers with different colors in the plot indicate the slopes of curves in power-law shear thinning regions. (b) Plots of p_x and S_d as a function of shear rate for the R_6C_4, R_6C_8, and R_6C_{10} diblock copolymer solutions.

samples of R_6C_4, R_6C_8, and R_6C_{10} solutions were examined. Their flow curves exhibit shear thinning fluid characteristics, as shown in Figure 7(a). The viscosity-shear rate curves can also be divided into three regions of shear thinning I, platform region II, and shear thinning III. The slopes of all the three curves in the region I are approximately the same closing to −0.35, while they are −0.18, −0.25, and −0.29 in the region III for R_6C_4, R_6C_8, and R_6C_{10}, respectively. The stretching degree of coil blocks S_d and normalized length projection of rods along the flow direction p_x for R_6C_n solutions were plotted as a function of shear rate, which is shown in Figure 7(b). The orientation behaviors of rod blocks are almost the same, as the lengths of rod blocks are the same for the R_6C_n solutions. The stretching degrees of coil blocks maintain invariable in the region I and II, while change more dramatically as the length of coil blocks increases. Therefore, increasing the length of coil blocks exerts less marked influence on the slopes of curves in the regions I and II, but leads to the increase of slopes in the region III. In addition, the R_6C_n solutions with $\phi = 0.1$, $\phi = 0.2$, and $\phi = 0.3$ were also investigated. We observed that the systems with $\phi = 0.2$ and $\phi = 0.3$ show similar three-region behaviors but different slopes and region boundaries, while the system with $\phi = 0.1$ exhibits Newtonian fluid behaviors.

Figure 8(a) shows the viscosity-shear rate curves for the R_mC_4 solutions under steady shear flow. Four samples of R_6C_4, R_8C_4, $R_{10}C_4$, and $R_{12}C_4$ solutions were examined. The viscosity-shear rate curves are also divided into three regions,
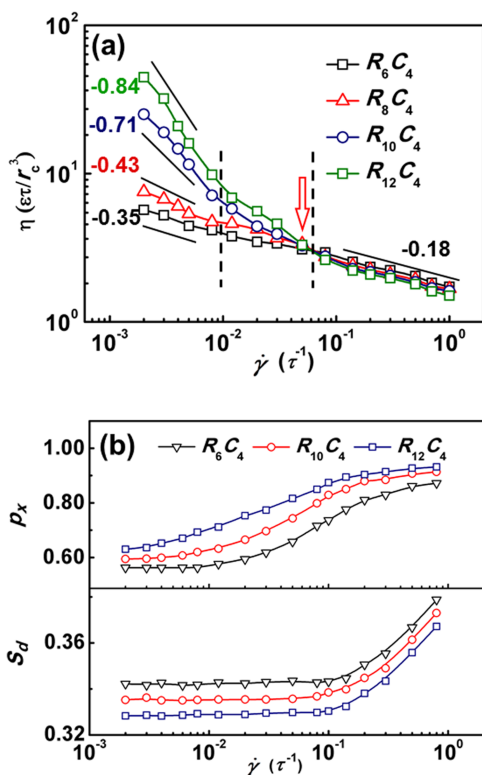

FIG. 8. (a) Shear viscosity as a function of the shear rate for the solutions of R_mC_4 diblock copolymers with various lengths of rod blocks at $\phi = 0.4$. The numbers with different colors in the plot indicate the slopes of curves in power-law shear thinning regions. The crossover of viscosity in the curves is marked by the red arrow. (b) Plots of p_x and S_d as a function of shear rate for the R_6C_4, $R_{10}C_4$, and $R_{12}C_4$ diblock copolymer solutions.

despite the absence of platform region in the systems with longer rod blocks. In the region I, it can be seen from Figure 8(a) that the viscosity of R_mC_4 solutions increases with increasing the length of rod blocks. The slopes of viscosity-shear rate curve are −0.35, −0.43, −0.70, and −0.84 for R_6C_4, R_8C_4, $R_{10}C_4$, and $R_{12}C_4$, respectively. The viscosity enhancement for R_mC_4 solutions having longer rod blocks originates from the weakening of the tumbling and flow ability as the length of blocks increases. Figure 8(b) shows the p_x and S_d as a function of shear rate for the R_mC_4 solutions. It was found that p_x started increasing at lower shear rate for longer rod blocks, which induces the shift to lower shear rate of the tumbling-alignment transition for longer rod blocks. Therefore, the viscosity-shear rate curves turn to be deeper for R_mC_4 solutions having longer rod blocks in the region I. The absence of shear platform in the region II for the solutions having longer rod blocks can be explained as follow. As mentioned above, in the region II, the increase of interfacial energy increases the resistance to shear flow and the loss of distortional elasticity reduces the resistance. However, the interfacial area of long rod block systems could not increase too much due to the stereoscopic effect, and thus the increase of resistance to shear flow could not balance the loss of the resistance by the loss of distortional elasticity. This leads to the gradually decrease of viscosity and the absence of the region II.

Interestingly, a crossover (marked by the red arrow in Figure 8(a)) is found at $\dot{\gamma} = 0.05\tau^{-1}$ in the viscosity-shear rate curves. The viscosity abnormally decreases with increasing the length of rod blocks in the region of $\dot{\gamma} > 0.05\tau^{-1}$. From Figure 8(b), it can be seen that the p_x increases with increasing the length of rod blocks in the region of $\dot{\gamma} > 0.05\tau^{-1}$, due to the stronger tendency to parallel align along the flow direction for the longer rod blocks under large shear rate. As a result, the slippage of longer rod blocks gets easier, leading to the decrease of viscosity for R_mC_4 solutions having longer rod blocks in the region III. In addition, as mentioned above, the S_d of coil blocks influences the rheological properties in the region III. As the lengths of coil blocks are the same in all the R_mC_4 solutions, the stretching degrees show almost the same variation tendency (see Figure 8(b)), and thus the slopes of viscosity-shear rate curves are approximately similar in the region III.

Some experiments were also conducted to study the rheological properties of rod-coil diblock copolymers,[6,19] supporting our theoretical results. Ober and co-authors reported that changing the molecular architecture from neat rigid homopolymer poly{2,5-(4-butylbenzoyl)oxystyrene} (PBBOS) to rod-coil diblock copolymer PBBOS-*b*-PS induces a decrease of the complex viscosity,[6] which confirms our results of Figure 6(a). Similar to our simulated results, the flow curve of homopolymer PBBOS also display three-region behaviors. However, the flow curves of PBBOS-*b*-PS do not present three-region behaviors. The main reason is that the viscous flow activation energy of PBBOS-*b*-PS is too low, so that the distortional elastic is not strong enough in the region I. Jeong and colleagues found that increasing the concentration of poly(ethylene glycol)-poly(*L*-alanine) (PEG-*L*-PA) leads to the gelation,[19] which qualitatively confirms our simulated results. The value of critical concentration in their

work is smaller than that in our simulations. This deviation is originated from the difference between the definition of concentration in simulations and experiments, the loss of molecular details in DPD, as well as the neglect of the entanglement and excluded-volume effects. They also showed that the sol-gel transition temperature of PEG-*L*-PA decreases with increasing the molecular weight ratio of the rod block to the coil block. Comparing Figure 7(a) with Figure 8(a) in our simulated results, one can observe that increasing the length of rod blocks enhances the viscosity more significantly than that of coil blocks, which is in coincidence with the Jeong's experimental results.

Beyond the reproductions of general features of experimental findings for the systems of rod-coil diblock copolymers in solutions, the simulations can reveal the microscopic origin of the complex rheological properties of polymeric systems and deepen the understanding of the experimental observations. In the simulations, it is convenient to visualize the molecular information and the orientation behaviors. For instance, the enlarged view of Figure 2(a) displays the packing of rod blocks and Figures 5–8 show the orientation behaviors of rod and coil blocks under shear flow, which are difficult to be deduced from the experiments. More importantly, it is convenient to calculate the dynamic parameters that can reveal the microscopic origin of the rheological properties. For example, the rotational relaxation time of rod blocks and the Rouse time of coil blocks are respectively deduced from the mean square displacement and the time correction function (Figure S2 of supplementary material). These time scales can be used to comprehend the crossovers in the three-region rheological behaviors of the rod-coil diblock copolymer solutions, which are different from that of the traditional flexible polymeric solutions and shows similarity to the lyotropic liquid crystal polymers.[14–16] In addition, we conducted some other systems with different molecular architectures, which further confirm the microscopic origin of the three-region behaviors in the shear flow.

Moreover, in this work, we interestingly found that the asymmetric rod-coil diblock copolymers with longer rod blocks and shorter coil blocks have the properties of enhanced distortion elastic properties at low shear rate and reduced shear viscosity at high shear rate. These solutions having asymmetric architecture rod-coil copolymers may find applications in biomedical technology, such as injective scaffold materials.[58] For clinic applications, these injective scaffold materials need high flow capacity at large shear rate that is helpful for injection. At rest state, however, these materials need enhanced mechanical property that is in favor of mechanical supports, resisting external pressure, and maintaining the original shape and integrity of organization. Therefore, the solutions having asymmetric rod-coil copolymers could meet the requirements of injective scaffold materials for clinic applications. In practice, our simulations help us get a deeper insight into the mechanisms of complex rheology of copolymers with different conformations. The simulated results could help for providing useful information for designing and fabricating advanced materials and understanding the relationship between gel structures and rheological properties.

IV. CONCLUSIONS

We utilized the non-equilibrium dissipative particle dynamics simulations to study the shear flow behavior of rod-coil diblock copolymers in selective solvents. The solutions with high copolymer concentrations present three-region behavior including shear thinning region I, platform region II, and shear thinning region III. It was found that the three-region behavior is governed by the differences in the time scale responding to the shear flow of rod and coil blocks. The tumbling-alignment transition of rod blocks is responsible for the region I and platform region II, while the stretching behavior of the coil blocks causes the power-law shear thinning in region III. Moreover, it was found that the viscosity increases with the length of rod blocks in the low-shear-rate region for the copolymers with same molecular weight. Our research revealed the microscopic origin of complex rheological properties of the rod-coil diblock copolymers in solutions and may provide useful information for preparing advanced gels or liquid crystals based on the rod-coil diblock copolymers.

SUPPLEMENTARY MATERIAL

See supplementary material for the temporal evolution of $u_x(t)$, MSD, and TCF.

ACKNOWLEDGMENTS

[1]M. Lee, B.-K. Cho, and W.-C. Zin, Chem. Rev. **101**, 3869–3892 (2001).
[2]A. P. Nowak, V. Breedveld, L. Pakstis, B. Ozbas, D. J. Pine, D. Pochan, and T. J. Deming, Nature **417**, 424–428 (2002).
[3]J.-H. Ryu, D.-J. Hong, and M. Lee, Chem. Commun. 1043–1054 (2008).
[4]A. C. Kamps, M. Fryd, and S.-J. Park, ACS Nano **6**, 2844–2852 (2012).
[5]J. F. Reuther, D. A. Siriwardane, R. Campos, and B. M. Novak, Macromolecules **48**, 6890–6899 (2015).
[6]P. Gopalan, Y. Zhang, X. Li, U. Wiesner, and C. K. Ober, Macromolecules **36**, 3357–3364 (2003).
[7]V. Breedveld, A. P. Nowak, J. Sato, T. J. Deming, and D. J. Pine, Macromolecules **37**, 3943–3953 (2004).
[8]M. Wang, K. Timachova, and B. D. Olsen, Macromolecules **48**, 3121–3129 (2015).
[9]J. D. Ferry, *Viscoelastic Properties of Polymers*, 3rd ed. (John Wiley & Sons, New York, 1980).
[10]R. B. Bird, R. C. Armstrong, and O. Hassager, *Dynamics of Polymeric Liquids. Volume 1: Fluid Mechanics* (Wiley, New York, 1987).
[11]M. Doi, J. Polym. Sci.: Polym. Phys. Ed. **19**, 229–243 (1981).
[12]R. G. Larson, Macromolecules **23**, 3983–3992 (1990).
[13]W. R. Burghardt and G. G. Fuller, J. Rheol. **34**, 959–992 (1990).
[14]W. R. Burghardt and K. Hongladarom, Macromolecules **27**, 2327–2329 (1994).
[15]K. Hongladarom, V. M. Ugaz, D. K. Cinader, W. R. Burghardt, J. P. Quintana, B. S. Hsiao, M. D. Dadmun, W. A. Hamilton, and P. D. Butler, Macromolecules **29**, 5346–5355 (1996).
[16]V. M. Ugaz, D. K. Cinader, and W. R. Burghardt, Macromolecules **30**, 1527–1530 (1997).
[17]S. Curgul and B. Erman, Polymer **46**, 275–281 (2005).
[18]B. D. Olsen, N. P. Teclemariam, S. J. Muller, and R. A. Segalman, Soft Matter **5**, 2453–2462 (2009).
[19]Y. Y. Choi, J. H. Jang, M. H. Park, B. G. Choi, B. Chi, and B. Jeong, J. Mater. Chem. **20**, 3416–3421 (2010).

[20]Y.-L. Lin, H.-Y. Chang, Y.-J. Sheng, and H.-K. Tsao, Soft Matter **9**, 4802–4814 (2013).

[21]K. Kremer and G. S. Grest, J. Chem. Phys. **92**, 5057–5086 (1990).

[22]A. Berker, S. Chynoweth, U. C. Klomp, and Y. Michopoulos, J. Chem. Soc., Faraday Trans. **88**, 1719–1725 (1992).

[23]H. Guo, K. Kremer, and T. Soddemann, Phys. Rev. E **66**, 061503 (2002).

[24]C.-L. Fu, Z.-Y. Sun, and L.-J. An, J. Phys. Chem. B **115**, 11345–11351 (2011).

[25]C.-L. Fu, X.-Z. Jia, Z.-Y. Sun, and L.-J. An, Polymer **55**, 4538–4545 (2014).

[26]X. Xu, J. Chen, and L. An, J. Chem. Phys. **140**, 174902 (2014).

[27]E. Hajizadeh, B. D. Todd, and P. J. Daivis, J. Chem. Phys. **141**, 194905 (2014).

[28]R. D. Groot and P. B. Warren, J. Chem. Phys. **107**, 4423–4435 (1997).

[29]P. J. Hoogerbrugge and J. M. V. A. Koelman, Europhys. Lett. **19**, 155–160 (1992).

[30]J. M. V. A. Koelman and P. J. Hoogerbrugge, Europhys. Lett. **21**, 363–368 (1993).

[31]R. D. Groot, T. J. Madden, and D. J. Tildesley, J. Chem. Phys. **110**, 9739–9749 (1999).

[32]M. A. Horsch, Z. Zhang, C. R. Iacovella, and S. C. Glotzer, J. Chem. Phys. **121**, 11455–11462 (2004).

[33]T. Soddemann, B. Dunweg, and K. Kremer, Phys. Rev. E **68**, 046702 (2003).

[34]I. Rychkov and K. Yoshikawa, J. Chem. Phys. **120**, 3482–3488 (2004).

[35]I. V. Pivkin and G. E. Karniadakis, J. Comput. Phys. **207**, 114–128 (2005).

[36]L.-Y. You, L.-J. Chen, H.-J. Qian, and Z.-Y. Lu, Macromolecules **40**, 5222–5227 (2007).

[37]D. A. Fedosov, G. E. Karniadakis, and B. Caswell, J. Chem. Phys. **132**, 144103 (2010).

[38]Y. R. Sliozberg, J. W. Andzelm, J. K. Brennan, M. R. Vanlandingham, V. Pryamitsyn, and V. Ganesan, J. Polym. Sci.: Part B: Polym. Phys. **48**, 15–25 (2010).

[39]Z. Zhang and H. Guo, J. Chem. Phys. **133**, 144911 (2010).

[40]T. Jiang, L. Wang, and J. Lin, Langmuir **29**, 12298–12306 (2013).

[41]A. Nikoubashman, R. L. Davis, B. T. Michal, P. M. Chaikin, R. A. Register, and A. Z. Panagiotopoulos, ACS Nano **8**, 8015–8026 (2014).

[42]L. S. Shagolsem, T. Kreer, and J.-U. Sommer, ACS Macro Lett. **3**, 1201–1204 (2014).

[43]S. Medina, J. Zhou, Z.-G. Wang, and F. Schmid, J. Chem. Phys. **142**, 024103 (2015).

[44]G. Jung and F. Schmid, J. Chem. Phys. **144**, 204104 (2016).

[45]L. S. Shagolsem, T. Kreer, A. Galuschko, and J.-U. Sommer, J. Chem. Phys. **145**, 164908 (2016).

[46]J. Liu, E. Sheina, T. Kowalewski, and R. D. McCullough, Angew. Chem., Int. Ed. **41**, 329–332 (2002).

[47]W. Ding, S. Lin, J. Lin, and L. Zhang, J. Phys. Chem. B **112**, 776–783 (2008).

[48]S. Lin, N. Numasawa, T. Nose, and J. Lin, Macromolecules **40**, 1684–1692 (2007).

[49]S. Lin, X. He, Y. Li, J. Lin, and T. Nose, J. Phys. Chem. B **113**, 13926–13934 (2009).

[50]C. Cai, L. Wang, J. Lin, and X. Zhang, Langmuir **28**, 4515–4524 (2012).

[51]C. Tsitsilianis, I. Iliopoulos, and G. Ducouret, Macromolecules **33**, 2936–2943 (2000).

[52]W. R. Burghandt, Macromol. Chem. Phys. **199**, 471–488 (1998).

[53]S. Liu, B. Ashok, and M. Muthukumar, Polymer **45**, 1383–1389 (2004).

[54]R. E. Teixeira, H. P. Babcock, E. S. G. Shaqfeh, and S. Chu, Macromolecules **38**, 581–592 (2005).

[55]R. G. Winkler, J. Chem. Phys. **133**, 164905 (2010).

[56]I. S. Dalal, N. Hoda, and R. G. Larson, J. Rheol. **56**, 305–332 (2012).

[57]M. Doi and S. F. Edwards, *The Theory of Polymer Dynamics* (Oxford University, Oxford, 1986).

[58]J. L. Drury and D. J. Mooney, Biomaterials **24**, 4337–4351 (2003).